Comparing parameterized and self-consistent approaches to ab inito CQED for electronic strong coupling

Ruby Manderna, Nam Vu, and Jonathan J. Foley IV*[a)]
Department of Chemistry, University of North Carolina Charlotte, 9201 University City Bldv, Charlotte, North Carolina 07470A

Molecules under strong or ultra-strong light-matter coupling present an intriguing route to modify chemical structure, properties, and reactivity. A rigorous theoretical treatment of such systems requires handling matter and photon degrees of freedom on an equal quantum mechanical footing. In the regime of molecular electronic strong or ultra-strong coupling to one or a few molecules, it is desirable to treat the molecular electronic degrees of freedom using the tools of ab initio quantum chemistry, yielding an approach referred to as ab initio cavity quantum electrodynamics (ai-QED), where the photon degrees of freedom are treated at the level of cavity quantum electrodynamics. In this letter, we analyze two complementary approaches to ai-QED: (1) parameterized CQED (pQED), a two-step approach where the matter degrees of freedom are computed using existing electronic structure theories, enabling the construction of rigorous ai-QED Hamiltonians in a basis of many-electron eigenstates, and (2) self-consistent CQED (scQED), a one-step approach where electronic structure methods are generalized to include coupling between electronic and photon degrees of freedom. Although these approaches are equivalent in their exact limits, we identify a disparity between the projection of the two-body dipole self-energy operator that appears in the pQED approach and its exact counterpart in the scQED approach. We provide a theoretical argument that this disparity resolves only under the limit of a complete orbital basis and a complete many-electron basis for the projection. We present numerical results highlighting this disparity and its resolution in simple molecular systems, where it is possible to approach these two complete basis limits simultaneously. Additionally, we examine and compare the practical issue of computational cost required to converge each approach towards the complete orbital and many-electron bases.

I. INTRODUCTION

Strong interactions between molecular electronic and photonic degrees of freedom (i.e., electronic strong and ultra-strong coupling) can fundamentally alter chemical structure, reactivity, and phenomenology.[1–23] Predictive theoretical and computational models for molecules under electronic strong coupling must capture the quantum nature of electronic and photonic degrees of freedom. In the limit of molecular electronic strong or ultra-strong coupling to one or a few molecules, it is desirable to treat the molecular electronic degrees of freedom using the tools of *ab initio* quantum chemistry, yielding an approach referred to as *ab initio* cavity quantum electrodynamics (ai-QED), where the photon degrees of freedom are treated at the level of cavity quantum electrodynamics. Two complementary approaches have emerged for ai-QED: (1) parameterized CQED[20,23–27] (pQED), a two-step approach where the matter degrees of freedom are computed using existing electronic structure theories, enabling one to build rigorous ai-QED Hamiltonians in a basis of many-electron eigenstates, and (2) self-consistent CQED[19,28–42] (scQED), a one-step approach where electronic structure methods are generalized to include coupling between electrons and photon degrees of freedom.

Although these approaches are equivalent in their exact limits, it is practically impossible to reach these exact limits for the vast majority of physicall relevant systems. Outside of their exact limits, the variety of approximations inherent in electronic structure calculations makes it quite difficult to assess these two approaches on equal footing. In this work, we attempt to provide a fair assessment of these two approaches based both upon simple analysis of their underlying formalism's, and through comparable numerical results that approach exact limits. To this end, we implement variational approaches to pQED and scQED using full configuration interaction (FCI) to parameterize the former and a self-consistent QED-FCI scheme for the latter.

II. VARIATIONAL AB INITIO QED

We will discuss two complementary variational approaches to ai-QED that seek to find accurate eigenstates of the Pauli-Fierz (PF) Hamiltonian[43,44] represented in the length gauge and within the dipole and Born-Oppenheimer approximations. Here we write down the Pauli-Fierz Hamiltonian for a molecular system coupled to a single photonic mode in atomic units as

$$\hat{H}_{\mathrm{PF}} = \hat{H}_e + \omega \hat{b}^\dagger \hat{b} - \sqrt{\frac{\omega}{2}} \hat{d}(\hat{b}^\dagger + \hat{b}) + \frac{1}{2}\hat{d}^2. \qquad (1)$$

In Eq. 1, $\hat{H}_e$ is the standard electronic Hamiltonian within the Born-Oppenheimer approximation[45], $\omega \hat{b}^\dagger \hat{b}$ is the bare Hamiltonian for the photon mode where ω represents the frequency and $\hat{b}^\dagger$ and $\hat{b}$ are raising and lower-

[a)]Electronic mail: jfoley19@charlotte.edu

ing operators for the photon mode. The final two terms capture interactions between the photonic and electronic degrees of freedom. In these interaction terms, known as the bilinear coupling and the quadratic dipole self energy, $\hat{d} = \boldsymbol{\lambda} \cdot \hat{\boldsymbol{\mu}}$ couples the field associated with the photon mode to the molecular dipole operator[46].

The formulation of several ai-QED methods (e.q. QED-Hartree–Fock, QED-CC, QED-CASCI) has been performed after transforming Eq. 1 to the coherent-state basis[36,40,47,48],

$$\hat{H}_{\mathrm{CS}} = \hat{H}_e + \omega \hat{b}^\dagger \hat{b} - \sqrt{\frac{\omega}{2}}[\hat{d}_e - \langle \hat{d}_e \rangle](\hat{b}^\dagger + \hat{b}) + \frac{1}{2}[\hat{d}_e - \langle \hat{d}_e \rangle]^2. \tag{2}$$

This follows from a unitary transformation of the Pauli-Fierz Hamiltonian,

$$\hat{H}_{\mathrm{CS}} = \hat{U}_{\mathrm{CS}} \hat{H}_{\mathrm{PF}} \hat{U}_{\mathrm{CS}}^\dagger, \tag{3}$$

where the Unitary coherent state transformation is defined as

$$\hat{U}_{\mathrm{CS}} = \exp\left(z(\hat{b}^\dagger - \hat{b})\right). \tag{4}$$

The parameter z may be computed as

$$z = \frac{-\langle \hat{d} \rangle}{\sqrt{2\omega}}. \tag{5}$$

Often, $\langle \hat{d} \rangle$ is computed for a given electronic reference state in, for example, the QED-HF reference in scQED formulations.[35,36] Here we will also investigate the CS transformation of the projected Pauli-Fierz Hamiltonian for a pQED formulation, where $\langle \hat{d} \rangle$ will be computed in the adiabatic many-electron basis. We note that within the Born-Oppenheimer approximation, the nuclear contribution in $\langle \hat{d} \rangle$ exactly cancels with the nuclear contribution to $\hat{d}$, hence we write Eq. 2 with $\hat{d}_e$ and $\langle \hat{d}_e \rangle$ to denote only the electronic contribution to both terms.

We can approach the variational solution to Eq. 1 or Eq. 2 in two complementary ways. The approach denoted pQED will first find the adiabatic eigenstates that define $\hat{H}_{\mathrm{e}}|\psi_\alpha(\mathbf{R})\rangle = E_\alpha(\mathbf{R})|\psi_\alpha(\mathbf{R})\rangle$ using standard quantum chemistry tools, where $\mathbf{R}$ denotes the coordinates of the nuclei which are fixed within the Born-Oppenheimer approximation. In a subsequent step, one builds a Hamiltonian matrix from Eq. 1 or Eq. 2 in the basis of direct products between these adiabatic eigenstates and photonic Fock states. The approach denoted scQED will seek the eigenstates of Eq. 1 or Eq. 2 directly in a product basis of many-electron states (here Slater determinants) and photonic Fock states.

Both approaches can reach an exact limit. For pQED, the exact limit can be achieved when one builds Eq. 1 or 2 in the complete basis of *exact* adiabatic eigenstates and photon number states. Of course, it is practically impossible to reach this limit for most molecular systems, so a practical variational approach will consider building the pQED Hamiltonian in a truncated basis of many-electron states. In practice, this basis of adiabatic eigenstates is not only incomplete, but the states themselves are inexact because they results from an approximate quantum chemistry method. The approximations inherent in practical quantum chemistry calculations include truncation of the single-particle basis (e.g. using a finite number of Gaussian-type orbital basis functions), and truncation of the many-electron space through, for example, truncation of the excitation rank in a configuration interaction (CI) ansatz. The exact limit of the scQED approach includes a complete single-particle basis for the electronic subsystem, a complete many-electron basis (through, e.g., a FCI ansatz that includes all excited electronic configurations, often represented as Slater determinants or configuration state functions), and a complete photon Fock space, which is also not practical in general. The practical limit of pCQED also includes the incomplete photon basis. Our goal in this current paper is to study the convergence properties of both methods towards their exact limits, and to point out quantitative differences that arise outside of the complete basis limit.

1. pQED

In the pQED approach, we can build Eq. 1 or 2 in a product basis of adiabatic electronic states and photonic Fock states, such that the coupled eigenstates can be expressed as linear combinations of these product basis states:

$$|\Psi_{\mathrm{ep}}\rangle = \sum_n \sum_\alpha C_{\alpha,n} |\psi_\alpha\rangle \otimes |n\rangle. \tag{6}$$

Here, the dependence of the adiabatic many-electron states on the nuclear coordinate $\mathbf{R}$ is implied. We briefly review the expressions that arise in the pQED approach leading to a matrix representation of Eq. 1 in a truncated basis of adiabatic electronic states; working equations for the matrix form of Eq. 2 will be provided in the supporting information. We can define a projection operator,

$$\hat{\mathcal{P}} = \sum_\alpha^N |\psi_\alpha\rangle\langle\psi_\alpha|, \tag{7}$$

that defines the truncation of the full electronic Hilbert space. We can also define the complementary projector $\hat{\mathcal{Q}}$ such that these two subspaces obey

$$\hat{\mathbf{1}} = \hat{\mathcal{P}} + \hat{\mathcal{Q}}, \tag{8}$$

where the resolution of the identity is satisfied by the complete electronic Hilbert space. Following the discussion by Huo and co-workers, we can think of the truncated version of Eq. 1 as arising from transformation with a projected Power-Zener-Woolley operator from the minimal coupling Hamiltonian[49]. From this perspective, we can write the projected Hamiltonian as follows:

$$\mathcal{H}_{PF} = \mathcal{H}_{\mathrm{e}} + \mathcal{H}_{\mathrm{cav}} + \mathcal{H}_{\mathrm{blc}} + \mathcal{H}_{\mathrm{dse}}, \tag{9}$$

where the caligraphic operators denote they have been projected into a subspace defined by $\hat{\mathcal{P}}$; that is, $\mathcal{H} = \hat{\mathcal{P}}\hat{H}\hat{\mathcal{P}}$. It is important to note that the projector only acts on matter operators, so we need only consider the impact of truncation on $\hat{H}_{\rm e}$, $\hat{H}_{\rm blc}$, and $\hat{H}_{\rm dse}$. The projected molecular electronic Hamiltonian has the form

$$\hat{\mathcal{P}}\hat{H}_{\rm e}\hat{\mathcal{P}} = \sum_{\alpha} E_\alpha |\psi_\alpha\rangle\langle\psi_\alpha| \tag{10}$$

where $E_\alpha = E_\alpha(\mathbf{R})$ are the energy eigenvalues of the adiabatic eigenstates noted in Eq. 6. The bilinear coupling terms has the form

$$\begin{aligned}\hat{\mathcal{P}}\hat{H}_{\rm blc}\hat{\mathcal{P}} &= -\sqrt{\frac{\omega}{2}}\hat{\mathcal{P}}\hat{d}\hat{\mathcal{P}}\left(\hat{b}^\dagger + \hat{b}\right) \\ &= -\sqrt{\frac{\omega}{2}}\sum_{\alpha\beta} d_{\alpha\beta}|\psi_\alpha\rangle\langle\psi_\beta|\left(\hat{b}^\dagger + \hat{b}\right),\end{aligned} \tag{11}$$

where $d_{\alpha\beta} = \langle\psi_\alpha|\hat{d}|\psi_\beta\rangle$ results from dotting the coupling vector into the transition dipole moment between adiabatic states α and β or the total dipole moment of state α when $\alpha = \beta$; this quantity also depends explicitly on the nuclear coordinates, but we are suppressing the dependence on $\mathbf{R}$ in our notation for simplicity. The transition dipole moments are purely electronic, while the total dipole moments have both an electronic and nuclear contribution. Finally, the dipole self energy has the form

$$\begin{aligned}\hat{\mathcal{P}}\hat{H}_{\rm dse}\hat{\mathcal{P}} &= \frac{1}{2}\hat{\mathcal{P}}\hat{d}\hat{\mathcal{P}}\hat{\mathcal{P}}\hat{d}\hat{\mathcal{P}} \\ &= \frac{1}{2}\sum_{\alpha\beta\gamma} d_{\alpha\gamma}d_{\gamma\beta}|\psi_\alpha\rangle\langle\psi_\beta|.\end{aligned} \tag{12}$$

If we build a matrix from the projected Pauli-Fierz matrix (here denoted $\mathcal{H}_{\rm pPF}$) in the basis given in Eq. 6, we have the general structure

$$\mathcal{H}_{\rm pPF} = \begin{bmatrix} \mathbf{E}+\mathbf{D} & \mathbf{d} & 0 & \dots & 0 & 0 \\ \mathbf{d} & \mathbf{E}+\mathbf{D}+\mathbf{\Omega} & \sqrt{2}\mathbf{d} & \dots & 0 & 0 \\ 0 & \sqrt{2}\mathbf{d} & \mathbf{E}+\mathbf{D}+2\mathbf{\Omega} & \dots & 0 & 0 \\ \vdots & \vdots & \vdots & \ddots & \vdots & \vdots \\ 0 & 0 & 0 & \dots & \mathbf{E}+\mathbf{D}+(N-1)\mathbf{\Omega} & \sqrt{N}\mathbf{d} \\ 0 & 0 & 0 & \dots & \sqrt{N}\mathbf{d} & \mathbf{E}+\mathbf{D}+N\mathbf{\Omega} \end{bmatrix}. \tag{13}$$

Here the elements of $\mathbf{E}$ are given by

$$\begin{aligned}E_{\alpha n,\beta m} &= \langle n|\langle\psi_\alpha|\mathcal{H}_{\rm e}|\psi_\beta\rangle|m\rangle \\ &= E_\alpha\delta_{\alpha\beta}\delta_{nm},\end{aligned} \tag{14}$$

the elements of $\mathbf{D}$ are

$$\begin{aligned}D_{\alpha n,\beta m} &= \langle n|\langle\psi_\alpha|\mathcal{H}_{\rm dse}|\psi_\beta\rangle|m\rangle \\ &= \frac{1}{2}\sum_{\gamma} d_{\alpha\gamma}d_{\gamma\beta}\delta_{nm},\end{aligned} \tag{15}$$

the elements of $\mathbf{d}$ are

$$\begin{aligned}d_{\alpha n,\beta m} &= \langle n|\langle\psi_\alpha|\mathcal{H}_{\rm blc}|\psi_\beta\rangle|m\rangle \\ &= -\sqrt{\frac{\omega}{2}}d_{\alpha\beta}\eta_{nm}\end{aligned} \tag{16}$$

where $\eta_{nm} = \sqrt{m+1}\delta_{n,m+1} + \sqrt{m}\delta_{n,m-1}$. The elements of $\mathbf{\Omega}$ are

$$\begin{aligned}\Omega_{\alpha n,\beta m} &= \langle n|\langle\psi_\alpha|\mathcal{H}_{\rm cav}|\psi_\beta\rangle|m\rangle \\ &= m\omega\delta_{\alpha\beta}.\end{aligned} \tag{17}$$

The structure of the matrix in Eq. 13 reflects the Kronecker delta functions that appear in the respective block equations.

A. scQED

In the self-consistent approach, one adapts their quantum chemistry method to directly include the terms beyond $\hat{H}_{\rm e}$ in Eq. 1. In this approach, we begin with the exact matter operators, which will be denoted in ordinary font, not caligraphic font like the projected matter operators in the previous subsection.

A variational scQED approach can be formulated based on the following configuration interaction ansatz

for the mixed electronic-photonic eigenstates:

$$|\Psi_{\rm ep}\rangle = \sum_n \sum_I C_{I,n} |\Phi_I\rangle \otimes |n\rangle, \tag{18}$$

where $|\Phi_I\rangle$ represents an electronic Slater determinant, $|n\rangle$ is a photon-number state corresponding to n photons in the cavity mode, and $C_{I,n}$ is an expansion coefficient[40]. Then, a variational scQED approach can be formulated as a matrix diagonalization problem where Eq. 1 is built in the basis of product states in Eq. 18. This matrix (here denoted $\mathbf{H}_{\rm PF-CI}$) has a similar structure as Eq. 13:

$$\mathbf{H}_{\rm PF-CI} = \begin{bmatrix} \mathbf{A}+\mathbf{\Delta} & \mathbf{G} & 0 & \dots & 0 & 0 \\ \mathbf{G} & \mathbf{A}+\mathbf{\Delta}+\mathbf{\Omega} & \sqrt{2}\mathbf{G} & \dots & 0 & 0 \\ 0 & \sqrt{2}\mathbf{G} & \mathbf{A}+\mathbf{\Delta}+2\mathbf{\Omega} & \dots & 0 & 0 \\ \vdots & \vdots & \vdots & \ddots & \vdots & \vdots \\ 0 & 0 & 0 & \dots & \mathbf{A}+\mathbf{\Delta}+(N-1)\mathbf{\Omega} & \sqrt{N}\mathbf{G} \\ 0 & 0 & 0 & \dots & \sqrt{N}\mathbf{G} & \mathbf{A}+\mathbf{\Delta}+N\mathbf{\Omega} \end{bmatrix}. \tag{19}$$

The elements of $\mathbf{A}$ are

$$\begin{aligned} A_{In,Jm} &= \langle n|\langle\Phi_I^{\rm e}|\hat{H}_{\rm e}|\Phi_J^{\rm e}\rangle|m\rangle \\ &= \langle\Phi_I^{\rm e}|\hat{H}_{\rm e}|\Phi_J^{\rm e}\rangle\delta_{nm}. \end{aligned} \tag{20}$$

The elements of $\mathbf{\Delta}$ are

$$\begin{aligned} \Delta_{In,Jm} &= \frac{1}{2}\langle n|\langle\Phi_I^{\rm e}|\hat{d}^2|\Phi_J^{\rm e}\rangle|m\rangle \\ &= \frac{1}{2}\left(\langle\Phi_I^{\rm e}|\hat{d_{\rm e}}^2|\Phi_J^{\rm e}\rangle + 2d_n\langle\Phi_I^{\rm e}|\hat{d}_{\rm e}|\Phi_J^{\rm e}\rangle + d_n^2\delta_{IJ}\right)\delta_{nm}, \end{aligned} \tag{21}$$

where $\hat{d}_{\rm e}$ denotes the electronic contribution to $\hat{d}$ and $d_{\rm n}$ denotes the nuclear contribution. The matrix elements of $\mathbf{G}$ are

$$\begin{aligned} G_{In,Jm} &= -\sqrt{\frac{\omega}{2}}\langle n|\langle\Phi_I^{\rm e}|\,\hat{d}\,(\hat{b}^\dagger+\hat{b})|\Phi_J^{\rm e}\rangle|m\rangle \\ &= -\sqrt{\frac{\omega}{2}}\langle\Phi_I^{\rm e}|\hat{d}|\Phi_J^{\rm e}\rangle\eta_{nm}. \end{aligned} \tag{22}$$

Finally, the elements of $\mathbf{\Omega}$ are given by

$$\Omega_{In,Jm} = \langle n^{\rm P}|\langle\Phi_I^{\rm e}|\omega\hat{b}^\dagger\hat{b}|\Phi_J^{\rm e}\rangle|m^{\rm P}\rangle = m\omega\delta_{IJ}\delta_{nm}. \tag{23}$$

More explicit expressions for these matrix elements, as well as those for the elements corresponding to Eq. 2, can be found in Ref.[40].

B. Dipole Self Energy in pCQED vs scQED

A key difference between practical implementations of pQED and scQED resides in the treatment of the dipole self energy, specifically arising from the product of electronic operators in $\hat{d_{\rm e}}^2$.

In the scQED approach, we are not starting with any specific state truncation in mind, and so our scQED Hamiltonian is written in terms of exact electronic operators. In first quantization, we can expand $\hat{d_{\rm e}}^2$ as

$$\hat{d_{\rm e}}^2 = \sum_{i\neq j} d_{\rm e}(i)\, d_{\rm e}(j) + \sum_i [d_{\rm e}(i)]^2. \tag{24}$$

where i and j represent different electronic coordinates; hence we see that the dipole self energy operator contains both a one-electron contribution and a two-electron contribution. The one-electron contribution can be recognized as the negative of the quadrupole operator multiplied by coupling vector components. A practical scQED approach will depend on introducing an orbital basis (e.g. an orthonormal spin orbital basis). In this case, we can write the right-hand side of Eq. 24 in second-quantized notation as

$$\hat{d_{\rm e}}^2 = \sum_{pqrs} d_{pq} d_{rs} \hat{a}_p^\dagger \hat{a}_r^\dagger \hat{a}_s \hat{a}_q - \sum_{pq} Q_{pq} \hat{a}_p^\dagger \hat{a}_q. \tag{25}$$

where $\hat{a}^\dagger$ and $\hat{a}$ represent fermionic creation and annihilation operators, respectively. The symbols d_{pq} and Q_{pq} represent modified electric dipole and electric quadrupole integrals. We can see that this form of the dipole self energy operator employed in the scQED approach maintains the exact structure to within the discretization error introduced by a finite orbital basis.

Let us turn to the projected dipole self energy operator that arises in pQED, which as we saw in Eq. 12, contains a product of projected modified dipole operators:

$$\begin{aligned} &\hat{\mathcal{P}}\hat{d}_{\rm e}\hat{\mathcal{P}}\hat{\mathcal{P}}\hat{d}_{\rm e}\hat{\mathcal{P}} \\ &= \sum_{\alpha\gamma\delta\beta} |\psi_\alpha\rangle\langle\psi_\alpha|\hat{d}_{\rm e}|\psi_\gamma\rangle\langle\psi_\gamma|\psi_\delta\rangle\langle\psi_\delta|\hat{d}_{\rm e}|\psi_\beta\rangle\langle\psi_\beta| \\ &= \sum_{\alpha\gamma\beta} |\psi_\alpha\rangle\langle\psi_\alpha|\hat{d}_{\rm e}|\psi_\gamma\rangle\langle\psi_\gamma|\hat{d}_{\rm e}|\psi_\beta\rangle\langle\psi_\beta| \\ &= \sum_{\alpha\gamma\beta} d_{\alpha\gamma} d_{\gamma\beta} |\psi_\alpha\rangle\langle\psi_\beta|. \end{aligned} \tag{26}$$

Notably, the projected dipole self energy is missing the quadrupole terms that are present in the exact dipole self energy operator. Thus, in addition to the discretization error that arises from a finite orbital basis, the exact structure of the dipole self energy is lost upon projection onto an incomplete electronic subspace. We will see that this generally leads to a different variational problem whereby the pQED energies can converge to a different ground state solution than the scQED.

We now show that this difference resolves itself in the limit of a complete orbital and many-electron basis. First, we will show that the quadrupole term in the exact dipole self energy operator vanishes in the limit of a complete orbital basis. As a first step, we utilize the anticommutation relations in the two-electron part of Eq. 25:

$$\begin{aligned}
&\sum_{pqrs} d_{pq} d_{rs} \hat{a}_p^\dagger \hat{a}_r^\dagger \hat{a}_s \hat{a}_q \\
&= -\sum_{pqrs} d_{pq} d_{rs} \hat{a}_p^\dagger [\delta_{qr} - \hat{a}_q \hat{a}_r^\dagger] \hat{a}_s \\
&= \sum_{pq} d_{pq} \hat{a}_p^\dagger \hat{a}_q \sum_{rs} d_{rs} \hat{a}_r^\dagger \hat{a}_s - \sum_{pqr} d_{pr} d_{rq} \hat{a}_p^\dagger \hat{a}_q. \qquad (27)
\end{aligned}$$

We can now substitute the last line of Eq. 27 into Eq. 25:

$$\begin{aligned}
\hat{d_{\mathrm{e}}}^2 &= \sum_{pq} d_{pq} \hat{a}_p^\dagger \hat{a}_q \sum_{rs} d_{rs} \hat{a}_r^\dagger \hat{a}_s \\
&\quad - \sum_{pq} \left(\sum_r d_{pr} d_{rq} + Q_{pq} \right) \hat{a}_p^\dagger \hat{a}_q \qquad (28)
\end{aligned}$$

As a second step, we can insert a resolution of the identity into $\sum_r d_{pr} d_{rq}$ when the orbital basis is complete, which gives

$$\sum_r^\infty d_{pr} d_{rq} = -Q_{pq}, \qquad (29)$$

which means that when the orbital basis is complete, the quadrupole contribution to the dipole self energy vanishes, and we have

$$\hat{d}_{\mathrm{e}}^2 = \sum_{pq} d_{pq} \hat{a}_p^\dagger \hat{a}_q \sum_{rs} d_{rs} \hat{a}_r^\dagger \hat{a}_s. \qquad (30)$$

Finally, we note that in the pQED approach, when the dipole self energy is projected onto an incomplete electronic subspace, the product of $\hat{d}$ operators is replaced by product of matrix elements of those operators. However, in the limit that the electronic subspace is complete, we have $\hat{\mathcal{P}} = \hat{1}$ and we resolve the projected dipole self energy into a product of $\hat{d}$ operators:

$$\hat{\mathcal{P}} \hat{d}_{\mathrm{e}} \hat{\mathcal{P}} \hat{\mathcal{P}} \hat{d}_{\mathrm{e}} \hat{\mathcal{P}} = \hat{\mathcal{P}} \hat{d}_{\mathrm{e}} \hat{d}_{\mathrm{e}} \hat{\mathcal{P}}. \qquad (31)$$

Thus we conclude that the exact and projected dipole self energy operators agree in the limit that both the complete orbital and many-electron basis limits have been reached.

III. RESULTS

A glossary of abbreviations and terms used to discuss the results is provided in Table I below.

pQED	General approach where Eq. 1 or 2 are built in a product basis of adiabatic electronic states and photonic Fock states
scQED	General approach where Eq. 1 or 2 are built in a product basis of Slater determinants and photonic Fock states
pPF(N_{el}, N_p)	Projection of Eq. 1 onto a basis of N_{el} adiabatic many electron states and N_p photonic Fock states
PF-FCI-N_p	Self-consistent variational solution to Eq. 1 in a product basis of all excited Slater determinants and N_p photonic Fock states
pCS(N_{el}, N_p)	Projection of Eq. 2 onto a basis of N_{el} adiabatic many electron states and N_p photonic Fock states
CS-FCI-N_p	Self-consistent variational solution to Eq. 2 in a product basis of all excited Slater determinants and N_p photonic Fock states
pRabi(N_{el}, N_p)	Projection of Eq. 1 without the dipole self energy term onto a basis of N_{el} adiabatic many electron states and N_p photonic Fock states
Rabi-FCI-N_p	Self-consistent variational solution to Eq. 2 without the dipole self energy in a product basis of all excited Slater determinants and N_p photonic Fock states

TABLE I. Glossary of acronyms used throughout this paper.

A. Helium Hydride ion (HeH^+)

HeH^+ is a 2-electron system that has a permanent ground-state dipole moment and a dipole-allowed optical transition ($S_0 \rightarrow S_2$ with transition energy of 26.1 eV), which will permit us to study the behavior of the dipole self-energy on the ground and polariton states using scQED and pQED approaches as we approach the complete basis limit. We optimize the geometry of this system at the FCI/cc-pVTZ level; at this level, the equilibrium bond length is approximately 0.776 Angstroms and the dipole moment has a magnitude of 1.73 Debye along the internuclear axis. We study the ground state and polariton states at the PF-FCI and pPF levels using cc-pVXZ basis sets, where X is D, T, and Q, to progress towards the complete orbital basis limit.

We first report the absolute energy error of the pPF(N_{el},10) relative to PF-FCI-10 for each basis set, where N_{el} is the number of many-electron basis states

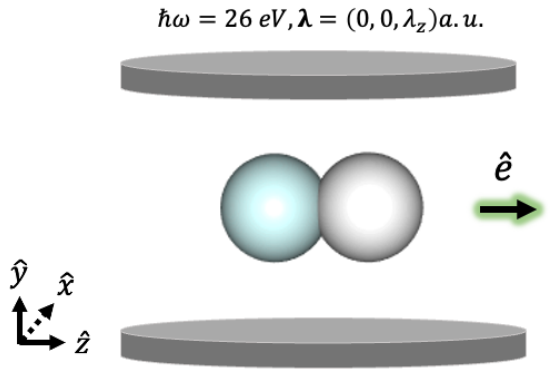

FIG. 1. Schematic of the HeH^+ coupled to a cavity mode polarized along the internuclear axis (z) and tuned to the first optically allowed transition from $S_0 \rightarrow S_2$ at approximately 26 eV.

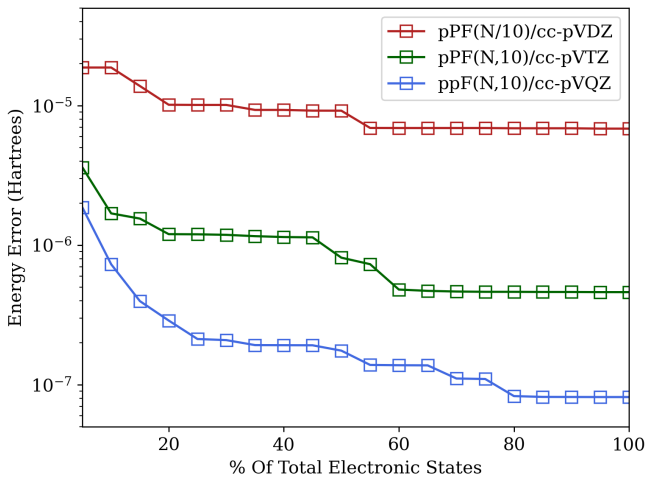

FIG. 2. Absolute error of pPF(N,10) relative to PF-FCI-10 computed within the cc-pVDZ, cc-pVTZ, and cc-pVQZ basis sets, where we plot this error as a function of the percentage of the FCI electronic states used to parameterize the pPF(N,10) method. The photon frequency in each case is tuned to the $S_0 \rightarrow S_2$ transition, and λ_z is fixed at 0.02 atomic units.

used to parameterize the pPF Hamiltonian see Figure 2). We find $N^{\mathrm{P}} = 10$ is sufficient to converge the photonic Fock space, and so PF-FCI-10 provides the exact energies for this system in a given orbital basis. We see that the energy error decreases as we increase N_{el} in a given orbital basis, and also decreases with increasing size of the orbital basis. The energy error of pPF(N_{el},10)/cc-pVDZ converges to ∼10 microHartrees in the limit that all of the FCI states are used to parameterize the Hamiltonian, while the energy error of pPF(N_{el},10)/cc-pVQZ converges to 0.1 microHartrees in the comparable limit (see Figure 2). The fraction of electronic states needed for energy convergence increases from around 50 percent in cc-pVDZ to 80 percent in cc-pVQZ. These results are consistent with the argument that the projected dipole self approaches the exact dipole self-energy in the limit that both the orbital and many-electron basis are complete.

Similarly, In Figure 3, the curves represent the absolute energy error vs coupling strength of the pPF(N_{el},10) ground-states in each basis set, where we have fixed N_{el} at the value where we observed the energy converge in Figure 2. All methods show errors of less than a microHartree for coupling strengths smaller than ∼0.01 atomic units but show increasing errors as the coupling strength increases. For pPF(2880,10)/cc-pVQZ, we see microHartree error with the largest coupling strength ($\lambda_z = 0.1$), and we see ∼100 microHartree error for pPF(60,10)/cc-pVDZ at this coupling strength. Because the dipole self-energy is quadratic in the coupling strength, we expect to see that the disparity between pQED and scQED will become more dramatic as the coupling strength increases. The progression shown in Figure 3 shows that differences between the exact and projected dipole self-energy operators have not been fully resolved even when using a cc-pVQZ orbital basis and 2880 many-electron states.

In Figures 4, 5, and 6, we show both ground state and polariton excitation energies of the HeH^+ system

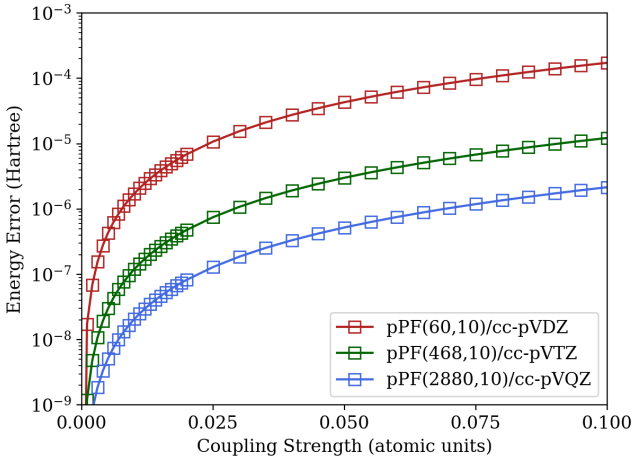

FIG. 3. Absolute error of pPF(N,10) relative to PF-FCI-10 computed within the cc-pVDZ, cc-pVTZ, and cc-pVQZ basis sets as a function of coupling strength. For each pPF(N,10) result, we choose N based on the smallest number of electronic states for which the energy error was converged with $\lambda_z = 0.02$ atomic units.

computed in all three basis sets with the pPF and PF-FCI approaches for varying values of coupling strength. The ground state energies are plotted relative to the uncoupled ground state, $E_{\mathrm{g}}(\lambda) - E_{\mathrm{g}}(\lambda = 0)$. The excitation energies are defined as the energy of a polariton state at a given coupling strength minus the ground state energy at the same coupling strength, $E_{\mathrm{pol}}(\lambda) - E_{\mathrm{g}}(\lambda)$. An interesting feature of this study is that the pPF (ground state and polariton) energies are consistently a lower bound on

the PF-FCI energies, and each approaches corresponding PF-FCI energy from below as we approach the complete basis limit. We emphasize that because the projected dipole self-energy is inexact outside of the complete basis limit, pPF and PF-FCI approaches provide a variational approach for two distinct Hamiltonians, and so we cannot make any concrete arguments about which should provide a lower bound in general. We do observe in these cases, that pPF(60,10)/cc-pVDZ ground-state and polariton energies are visibly lower than the PF-FCI-10/cc-pVDZ energies (see Figure 4). While the pPF(468,10)/cc-pVTZ and pPF(2880,10)/cc-pVQZ also provide ground state and polariton energies below their PF-FCI-10 counterparts, the difference is not visibly discernible (see Figures 5 and 6). We also note that progression of the Rabi splitting with increasing coupling strength is very comparable between the pPF and PF-FCI results for all basis sets. We expect that both methods should agree specifically in the Rabi splitting because this feature of the polariton states is dominated by the bilinear coupling, and the projected bilinear coupling remains the same form as it's exact counterpart.

Now that we have shown how the disparity between the pQED and scQED resolves in the complete basis set limit, we can ask a pragmatic question of which requires less computational effort to converge. For this comparison, we use the same direct CI algorithm for the scQED energies as we do for for the N_{el} energies and dipole moments required for the pQED results. Although we are typically only interested in a few low-energy eigenstates of Eq. 1 or Eq. 2, as we saw in Figure 2, one often needs to project the pPF Hamiltonian on many more states than the number of eigenstates that are of interest when the coupling is strong. Because the scQED approach solves Eq. 1 or Eq. 2 directly in a coupled basis, we need only solve for the number of roots of interest. The germane question is then how does the effort of solving for the N_{el} adiabatic states required for the lowest N_{ep} coupled states from pQED compare to directly solving for the lowest coupled N_{ep} states from scQED.

In Table II, we report the timings to solve for $N_{ep} = 10$ coupled states of HeH^+ under the same conditions as in Figure 2 using PF-FCI-10/cc-pVXZ compared to the time required to solve for $N_{el} = 40$, 312, and 1296 states at the FCI/cc-pVDZ, FCI/cc-pVTZ, and FCI/cc-pVQZ levels. We choose these N_{el} as 40% of the total roots of the FCI matrix at each basis set, which is approaching the upper limit of what can be performed with our direct CI approach. We note that for the study in Figure 2, we performed full diagonalization of each FCI matrix, not direct CI; this is because the iterative eigensolver used in the direct CI approach generally becomes unsuitable for finding 50% or more of the total eigenvalues of a given matrix. We see that in the cc-pVDZ basis set, it is faster to compute the lowest 40 roots of the FCI matrix than to compute the lowest 10 coupled states. However, the time required for finding the FCI roots increases by roughly 2 orders of magnitude as we progress from cc-pVDZ to cc-pVTZ and again to cc-pVQZ, whereas the time to solve for the lowest 10 coupled PF-FCI roots increases by only 1 order of magnitude for the same progression. Thus, we see it is approximately 10x faster to find the lowest 10 roots with PF-FCI-10/cc-pVTZ as compared to finding 312 FCI/cc-pVTZ roots, and it is approximately 100x faster to find the lowest 10 roots with PF-FCI-10/cc-pVQZ than to find the lowest 1296 FCI/cc-pVQZ roots.

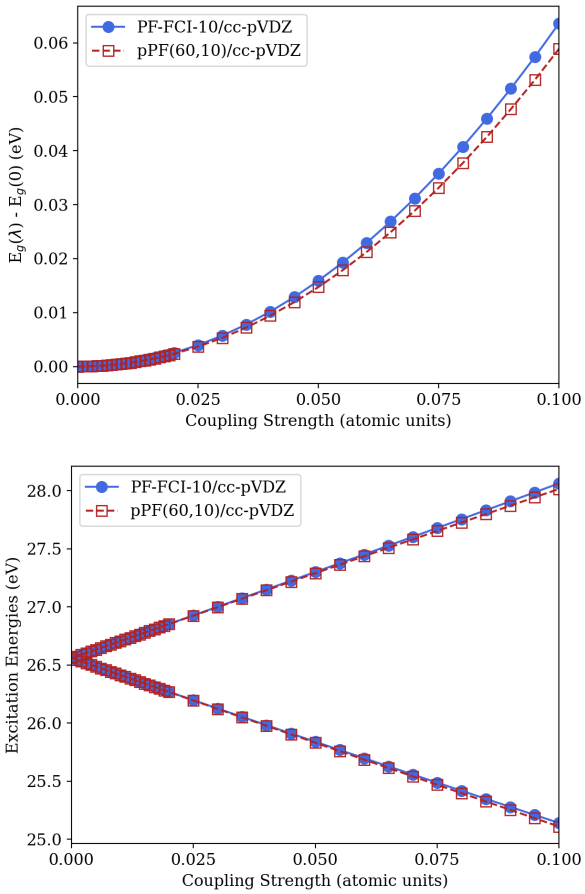

FIG. 4. Relative energy of the ground-state and excitation energies of polariton states of HHe^+ as a function of coupling strength computed at the PF-FCI-10/cc-pVDZ and pPF(60,10)/cc-pVDZ levels.

B. Lithium hydride (LiH)

The LiH molecule provides a 4-electron system that has a permanent ground-state dipole moment and a dipole-allowed optical transition ($S_0 \rightarrow S_1$ with transition energy of 3.29 eV). Although we can no longer afford to perform full diagonalization to obtain all FCI many-electron states for the cc-pVXZ series, we can perform FCI (and QED-FCI) in a split-valence triple zeta basis set (6-311G) and obtain hundreds of many-electron states. We will use

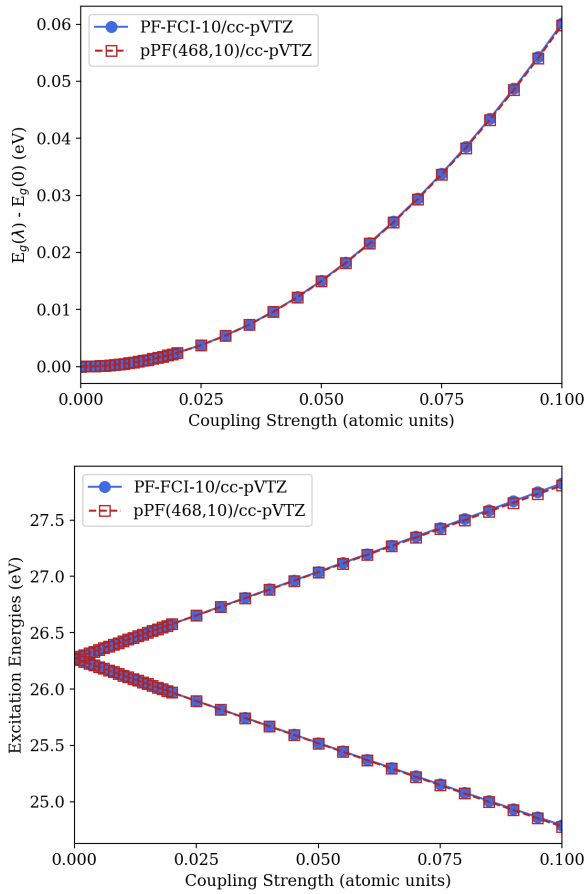

FIG. 5. Relative energy of the ground-state and excitation energies of polariton states of HHe^+ as a function of coupling strength computed at the PF-FCI-10/cc-pVTZ and pPF(468,10)/cc-pVTZ levels

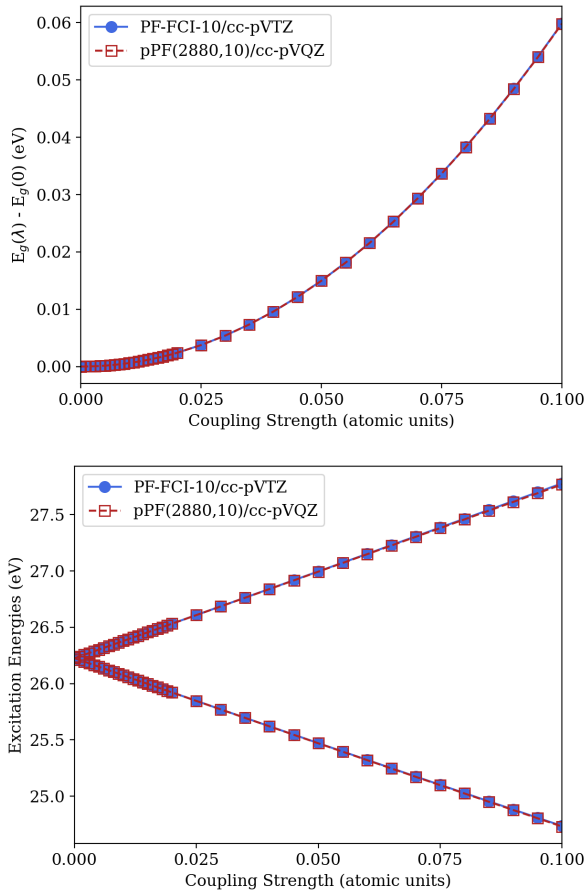

FIG. 6. Relative energy of the ground-state and excitation energies of polariton states of HHe^+ as a function of coupling strength computed at the PF-FCI-10/cc-pVQZ and pPF(2880,10)/cc-pVQZ levels

The figure key pVTZ should be changed to pVQZ

		PF-FCI		pPF
Basis Set	N_p	$t_{convergence}$ (s)	N_{el}	$t_{convergence}$
cc-pVDZ	10	$3.4 \cdot 10^{-2}$	40	$2.4 \cdot 10^{-2}$
cc-pVTZ	10	$4.2 \cdot 10^{-1}$	312	$3.5 \cdot 10^{0}$
cc-pVQZ	10	$9.2 \cdot 10^{0}$	1296	$4.0 \cdot 10^{2}$

TABLE II. Comparison of the time to converge the Davidson iterations for the coupled electronic-photonic roots of the PF-FCI method and the FCI electronic roots of the pPF method for cc-pVDZ, cc-pVTZ, and cc-pVQZ basis sets. For each pPF case, we converge N_{el} roots chosen to be 40% of the total number of FCI states in that basis. For each PF-FCI case, we solve for the lowest 10 coupled roots with a photonic Fock space that includes $n = 0, 1, ..., 10$.

this system to illustrate the behavior of the pQED and scQED methods in incomplete orbital and many-electron basis limits under strong coupling with $\boldsymbol{\lambda} = (0, 0, 0.05)$ atomic units.

We first compute the ground state potential energy scan of HF LiH? at the pPF(500,2)/6-311G,

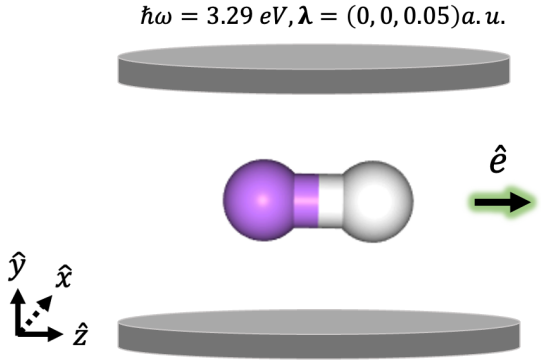

FIG. 7. Schematic of the LiH coupled to a cavity mode polarized along the internuclear axis (z) and tuned to the first optically allowed transition from $S_0 \rightarrow S_1$ at approximately 3.29 eV.

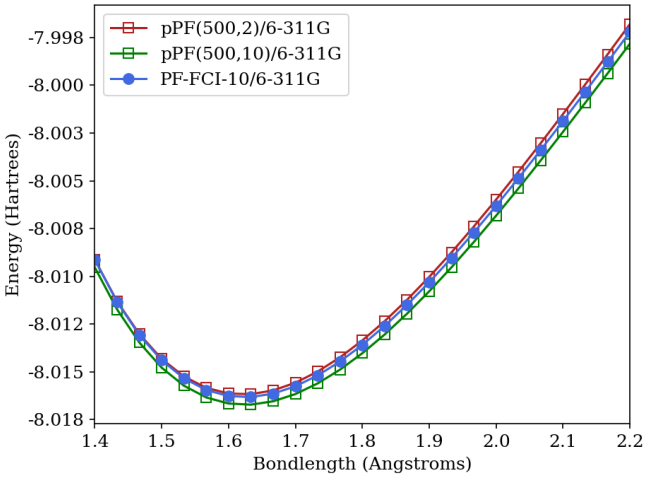

FIG. 8. The ground-state potential energy scan of LiH coupled to a cavity mode with $\lambda = (0, 0, 0.05)$ a.u. and ($\hbar\omega = 3.29eV$ at the pPF(500,2)/6-311G, pPF(500,10)/6-311G, and PF-FCI-10/6-311G levels.

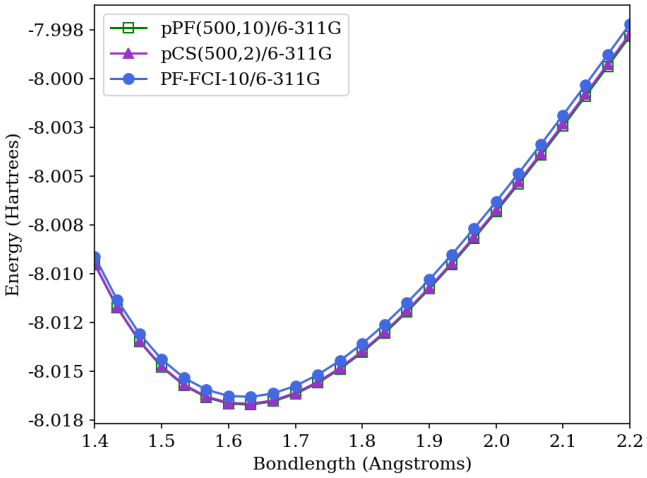

FIG. 9. The ground-state potential energy scan of LiH coupled to a cavity mode with $\lambda = (0, 0, 0.05)$ a.u. and ($\hbar\omega = 3.29eV$ at the pPF(500,10)/6-311G, pCS(500,2)/6-311G, and PF-FCI-10/6-311G levels.

pPF(500,10)/6-311G, where the latter is fully converged with respect to the size of the electronic and photonic spaces. While we again see that the pPF(500,10)/6-311G energies are a lower bound to the PF-FCI-10/6-311G energies, we see that the pPF(500,2)/6-311G energies are an upper bound to the pPF-FCI-10/6-311G energies (see Figure 8). This suggests that the photonic Fock space is incomplete in the latter case. In prior work on scQED approaches, we showed that scQED approaches based on Eq. 2 lead to faster convergence of the photonic Fock space. In Figure 9 we consider the same potential energy scan and compare the pCS(500,2)/6-311G

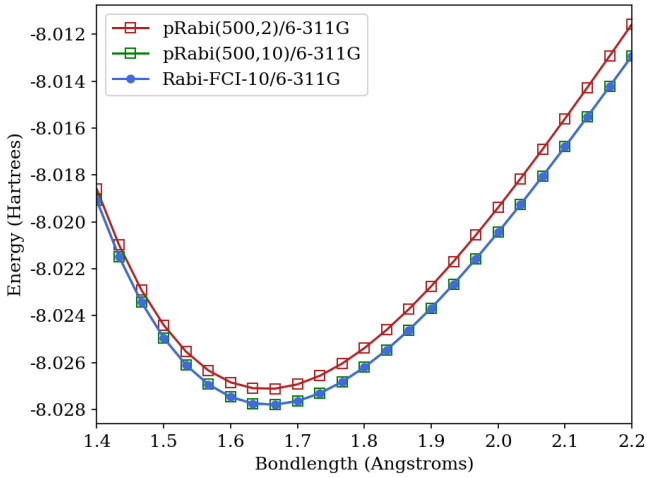

FIG. 10. The ground-state potential energy scan of LiH coupled to a cavity mode with $\lambda = (0, 0, 0.05)$ a.u. and ($\hbar\omega = 3.29eV$ at the pRabi(500,2)/6-311G, pRabi(500,10)/6-311G, and Rabi-FCI-10/6-311G levels.

and pPF(500,10)/6-311G levels to pPF-FCI-10/6-311G. In this case, we see that the pCS(500,2)/6-311G energies are indistinguishable from the pPF(500,10)/6-311G energies, suggesting that the same convergence of the photonic Fock space can be realized from the coherent state transformation in pQED approaches as has been observed in scQED approaches.

Finally, we perform the same scan with pQED and scQED approaches that neglect the dipole self energy operator altogether, which we term pRabi and Rabi-FCI approaches, respectively, to denote the analogy to the Rabi Hamiltonian. In these approaches, the only coupling between the electronic and photonic degrees of freedom arises through the bilinear coupling term. We compute the coupled LiH scan at the pRabi(500,2)/6-311G, pRabi(500,10)/6-311G, and Rabi-FCI-10/6-311G levels. Here we see that the the pRabi(500,2) results are an upper bound to both the pRabi(500,10) and Rabi-FCI-10 results, which again suggests an incomplete photonic Fock space. However, unlike the pPF and PF-FCI results we have examined so far, the pRabi and Rabi-FCI results are indistinguishable in the limit of a complete photonic Fock space. This is consistent with the proposition that the projected bilinear coupling operator agrees with the exact counterpart in a given orbital basis as long as it is projected onto a complete many-electron subspace.

IV. CONCLUDING REMARKS

In this work, we have provided a theoretical and numerical comparison of two complementary approaches to ai-QED: (1) parameterized CQED (pQED), a two-step approach where the matter degrees of freedom are computed using existing electronic structure theories, en-

abling one to build rigorous ai-QED Hamiltonians in a basis of many-electron eigenstates, and (2) self-consistent CQED (scQED), a one-step approach where electronic structure methods are generalized to include coupling between electrons and photon degrees of freedom. Using simple theoretical arguments, we have identified a disparity between the projection of the two-body dipole self energy operator that appears in the pQED approach and its exact operator counterpart in the scQED approach. We provided a simple theoretical argument that this disparity resolves only under the limit of a complete orbital basis and in the limit of a complete many-electron basis for the projection. We provided numerical results highlighting this disparity and its resolution on simple molecular systems where it is possible to approach these two complete basis limits simultaneously. We also examined and compared the practical issue of computational cost to converge each approach towards the complete orbital and many-electron bases.

Acknowledgments JJF and RM gratefully acknowledge the NSF CAREER Award CHE-2043215. JJF, RM, and NV acknowledges support from the Center for MAny-Body Methods, Spectroscopies, and Dynamics for Molecular POLaritonic Systems (MAPOL) under subcontract from FWP 79715, which is funded as part of the Computational Chemical Sciences (CCS) program by the U.S. Department of Energy, Office of Science, Office of Basic Energy Sciences, Division of Chemical Sciences, Geosciences and Biosciences at Pacific Northwest National Laboratory (PNNL). PNNL is a multi-program national laboratory operated by Battelle Memorial Institute for the United States Department of Energy under DOE contract number DE-AC05-76RL1830.

[1] A. Frisk Kockum, A. Miranowicz, S. De Liberato, S. Savasta, and F. Nori, "Ultrastrong coupling between light and matter," Nature Reviews Physics **1**, 19–40 (2019).

[2] J. Flick, N. Rivera, and P. Narang, "Strong light-matter coupling in quantum chemistry and quantum photonics," Nanophotonics **7**, 1479 – 1501 (2018).

[3] P. Törmä and W. L. Barnes, "Strong coupling between surface plasmon polaritons and emitters: a review," Reports on Progress in Physics **78**, 013901 (2014).

[4] D. G. Lidzey, D. D. C. Bradley, M. S. Skolnick, T. Virgili, S. Walker, and D. M. Whittaker, "Strong exciton–photon coupling in an organic semiconductor microcavity," Nature **395**, 53–55 (1998).

[5] J. Bellessa, C. Bonnand, J. C. Plenet, and J. Mugnier, "Strong coupling between surface plasmons and excitons in an organic semiconductor," Phys. Rev. Lett. **93**, 036404 (2004).

[6] J. A. Hutchison, T. Schwartz, C. Genet, E. Devaux, and T. W. Ebbesen, "Modifying chemical landscapes by coupling to vacuum fields," Angewandte Chemie International Edition **51**, 1592–1596 (2012).

[7] D. M. Coles, Y. Yang, Y. Wang, R. T. Grant, R. A. Taylor, S. K. Saikin, A. Aspuru-Guzik, D. G. Lidzey, J. K.-H. Tang, and J. M. Smith, "Strong coupling between chlorosomes of photosynthetic bacteria and a confined optical cavity mode," Nature Communications **5**, 5561 (2014).

[8] E. Orgiu, J. George, J. A. Hutchison, E. Devaux, J. F. Dayen, B. Doudin, F. Stellacci, C. Genet, J. Schachenmayer, C. Genes, G. Pupillo, P. Samorì, and T. W. Ebbesen, "Conductivity in organic semiconductors hybridized with the vacuum field," Nature Materials **14**, 1123–1129 (2015).

[9] R. Chikkaraddy, B. de Nijs, F. Benz, S. J. Barrow, O. A. Scherman, E. Rosta, A. Demetriadou, P. Fox, O. Hess, and J. J. Baumberg, "Single-molecule strong coupling at room temperature in plasmonic nanocavities," Nature **535**, 127–130 (2016).

[10] T. W. Ebbesen, "Hybrid light–matter states in a molecular and material science perspective," Accounts of Chemical Research **49**, 2403–2412 (2016).

[11] M. Sukharev and A. Nitzan, "Optics of exciton-plasmon nanomaterials," Journal of Physics: Condensed Matter **29**, 443003 (2017).

[12] X. Zhong, T. Chervy, L. Zhang, A. Thomas, J. George, C. Genet, J. A. Hutchison, and T. W. Ebbesen, "Energy transfer between spatially separated entangled molecules," Angewandte Chemie International Edition **56**, 9034–9038 (2017).

[13] K. Chevrier, J. M. Benoit, C. Symonds, S. K. Saikin, J. Yuen-Zhou, and J. Bellessa, "Anisotropy and controllable band structure in suprawavelength polaritonic metasurfaces," Phys. Rev. Lett. **122**, 173902 (2019).

[14] S. Kéna-Cohen and S. R. Forrest, "Room-temperature polariton lasing in an organic single-crystal microcavity," Nature Photonics **4**, 371–375 (2010).

[15] J. Lather, P. Bhatt, A. Thomas, T. W. Ebbesen, and J. George, "Cavity catalysis by cooperative vibrational strong coupling of reactant and solvent molecules," Angewandte Chemie International Edition **58**, 10635–10638 (2019).

[16] C. Climent, J. Galego, F. J. Garcia-Vidal, and J. Feist, "Plasmonic nanocavities enable self-induced electrostatic catalysis," Angewandte Chemie International Edition **58**, 8698–8702 (2019).

[17] R. K. Yadav, M. Otten, W. Wang, C. L. Cortes, D. J. Gosztola, G. P. Wiederrecht, S. K. Gray, T. W. Odom, and J. K. Basu, "Strongly coupled exciton–surface lattice resonances engineer long-range energy propagation," Nano Letters **20**, 5043–5049 (2020).

[18] B. Munkhbat, M. Wersäll, D. G. Baranov, T. J. Antosiewicz, and T. Shegai, "Suppression of photo-oxidation of organic chromophores by strong coupling to plasmonic nanoantennas," Science Advances **4**, eaas9552 (2018).

[19] A. E. DePrince III, "Cavity-modulated ionization potentials and electron affinities from quantum electrodynamics coupled-cluster theory," J. Chem. Phys. **154**, 094112 (2021).

[20] A. Mandal, M. Taylor, B. Weight, E. Koessler, X. Li, and P. Huo, "Theoretical advances in polariton chemistry and molecular cavity quantum electrodynamics," Chem. Rev. **16**, 9786–9879 (2023).

[21] F. Pavošević, S. Hammes-Schiffer, A. Rubio, and J. Flick, "Cavity-modulated proton transfer reactions," J. Am. Chem. Soc. **144**, 4995 (2022).

[22] "Molecular orbital theory in cavity qed environments," Nat. Commun. **13**, 1368 (2022).

[23] B. M. Weight, D. J. Weix, Z. J. Tonzetich, T. D. Krauss, and P. Huo, "Cavity quantum electrodynamics enables para- and ortho-selective electrophilic bromination of nitrobenzene," Journal of the American Chemical Society **0**, null (0), pMID: 38814893, https://doi.org/10.1021/jacs.4c04045.

[24] D. Hu and P. Huo, "Ab initio molecular cavity quantum electrodynamics simulations using machine learning models," J. Chem. Theory. Comput. **19**, 2353–2368 (2023), pMID: 37000936.

[25] B. M. Weight, T. D. Krauss, and P. Huo, "Investigating molecular exciton polaritons using ab initio cavity quantum electrodynamics," J. Phys. Chem. Lett. **14**, 5901–5913 (2023), pMID: 37343178.

[26] J. D. Weidman, M. S. Dadgar, Z. J. Stewart, B. G. Peyton, I. S. Ulusoy, and A. K. Wilson, "Cavity-modified molecular dipole switching dynamics," The Journal of Chemical Physics **160**, 094111 (2024), https://pubs.aip.org/aip/jcp/article-pdf/doi/10.1063/5.0188471/19708269/094111_1_5.0188471.pdf.

[27]B. G. Peyton, J. D. Weidman, and A. K. Wilson, "Light-induced electron dynamics of molecules in cavities: comparison of model hamiltonians," J. Opt. Soc. Am. B **41**, C74–C81 (2024).
[28]M. Ruggenthaler, F. Mackenroth, and D. Bauer, "Time-dependent Kohn-Sham approach to quantum electrodynamics," Phys. Rev. A **84**, 042107 (2011).
[29]I. V. Tokatly, "Time-dependent density functional theory for many-electron systems interacting with cavity photons," Phys. Rev. Lett. **110**, 233001 (2013).
[30]M. Ruggenthaler, J. Flick, C. Pellegrini, H. Appel, I. V. Tokatly, and A. Rubio, "Quantum-electrodynamical density-functional theory: Bridging quantum optics and electronic-structure theory," Phys. Rev. A **90**, 012508 (2014).
[31]C. Pellegrini, J. Flick, I. V. Tokatly, H. Appel, and A. Rubio, "Optimized effective potential for quantum electrodynamical time-dependent density functional theory," Phys. Rev. Lett. **115**, 093001 (2015).
[32]J. Flick, C. Schäfer, M. Ruggenthaler, H. Appel, and A. Rubio, "Ab initio optimized effective potentials for real molecules in optical cavities: Photon contributions to the molecular ground state," ACS Photonics **5**, 992–1005 (2018).
[33]R. Jestädt, M. Ruggenthaler, M. J. T. Oliveira, A. Rubio, and H. Appel, "Light-matter interactions within the ehrenfest–maxwell–pauli–kohn–sham framework: fundamentals, implementation, and nano-optical applications," Advances in Physics **68**, 225–333 (2019).
[34]J. Flick and P. Narang, "Ab initio polaritonic potential-energy surfaces for excited-state nanophotonics and polaritonic chemistry," J. Chem. Phys. **153**, 094116 (2020).
[35]J. McTague and J. J. Foley IV, "Non-hermitian cavity quantum electrodynamics–configuration interaction singles approach for polaritonic structure with ab initio molecular hamiltonians," J. Chem. Phys. **156**, 154103 (2022).
[36]T. S. Haugland, E. Ronca, E. F. Kjønstad, A. Rubio, and H. Koch, "Coupled cluster theory for molecular polaritons: Changing ground and excited states," Phys. Rev. X **10**, 041043 (2020).
[37]U. Mordovina, C. Bungey, H. Appel, P. J. Knowles, A. Rubio, and F. R. Manby, "Polaritonic coupled-cluster theory," Physical Reviews Research **2**, 023262 (2020).
[38]J. Yang, Q. Ou, Z. Pei, H. Wang, B. Weng, Z. Shuai, K. Mullen, and Y. Shao, "Quantum-electrodynamical time-dependent density functional theory within gaussian atomic basis," J. Chem. Phys. **155**, 064107 (2021).
[39]J. Yang, Z. Pei, E. C. Leon, C. Wickizer, B. Weng, Y. Mao, Q. Ou, and Y. Shao, "Cavity quantum-electrodynamical time-dependent density functional theory within Gaussian atomic basis. II. Analytic energy gradient," J. Chem. Phys. **156**, 124104 (2022).
[40]N. Vu, D. Mejia-Rodriguez, N. P. Bauman, A. Panyala, E. Mutlu, N. Govind, and J. J. I. Foley, "Cavity quantum electrodynamics complete active space configuration interaction theory," Journal of Chemical Theory and Computation **20**, 1214–1227 (2024), pMID: 38291561, https://doi.org/10.1021/acs.jctc.3c01207.
[41]B. M. Weight, S. Tretiak, and Y. Zhang, "Diffusion quantum monte carlo approach to the polaritonic ground state," Phys. Rev. A **109**, 032804 (2024).
[42]Z.-H. Cui, A. Mandal, and D. R. Reichman, "Variational lang–firsov approach plus møller–plesset perturbation theory with applications to ab initio polariton chemistry," J. Chem. Theory Comput. **20**, 1143 (2024).
[43]H. Spohn, *Dynamics of charged particles and their radiation field* (Cambridge Univ. Press, Cambridge, 2004).
[44]M. Ruggenthaler, N. Tancogne-Dejean, J. Flick, H. Appel, and A. Rubio, "From a quantum-electrodynamical light–matter description to novel spectroscopies," Nature Reviews Chemistry **2**, 0118 (2018).
[45]A. Szabo and N. S. Ostlund, *Modern Quantum Chemistry: Introduction to Advanced Electronic Structure Theory*, 1st ed. (Dover Publications, Inc., Mineola, 1996).
[46]R. H. Myhre, T. J. A. Wolf, L. Cheng, S. Nandi, S. Coriani, M. Gühr, and H. Koch, "A theoretical and experimental benchmark study of core-excited states in nitrogen," J. Chem. Phys. **148**, 064106 (2018).
[47]J. J. Foley IV, J. McTague, and A. E. DePrince III, "*Ab initio* methods for polariton chemistry," Chem. Phys. Rev **4**, 041301 (2023).
[48]M. D. Liebenthal, N. Vu, and A. E. DePrince III, "Assessing the effects of orbital relaxation and the coherent-state transformation in quantum electrodynamics density functional and coupled-cluster theories," J. Phys. Chem. A **127**, 5264–5275 (2023).
[49]M. A. D. Taylor, A. Mandal, W. Zhou, and P. Huo, "Resolution of gauge ambiguities in molecular cavity quantum electrodynamics," Phys. Rev. Lett. **125**, 123602 (2020).